Eur. Phys. J. D **15**, 99–104 (2001)

THE EUROPEAN PHYSICAL JOURNAL D

EDP Sciences

On the Stark broadening of the He I 447.1 nm spectral line

V. Milosavljević[a] and S. Djeniže

Faculty of Physics, University of Belgrade, P.O.B. 368, Belgrade, Serbia, Yugoslavia

Received 20 February 2001 and Received in final form 25 April 2001

Abstract. Characteristics of the Stark broadened and overlapping 447.1 nm He I spectral line and its forbidden 447.0 nm components have been measured at electron densities between 4.4×10^{22} m^{-3} and 8.2×10^{22} m^{-3} and electron temperatures between 18 000 K and 33 000 K in plasmas created in five various discharge conditions using the low pressure pulsed arc as an optically thin plasma source operated in helium-nitrogen-oxygen gas mixture. Good agreement was found among our measured line characteristics and their existing calculated values, based on the quasistatic approximation. Possible influence of the singly ionized oxygen impurity atoms (O II) on the intensity values of the dip between allowed and forbidden components was found that can explain the disagreement among some existing experimental and calculated line characteristics data, at higher electron temperatures and densities. On the basis of the observed asymmetry of the 447.1 nm spectral line profile we have obtained the ion contribution parameter at 10^{22} m^{-3} electron density and 8 000 K electron temperature.

PACS. 52.70.Kz Optical (ultraviolet, visible, infrared) measurements – 32.70.Jz Line shapes, widths, and shifts – 32.70.-n Intensities and shapes of atomic spectral lines

1 Introduction

Spectral line broadening characteristics such as the line width and line center shift can be used for the cosmic and laboratory plasma diagnostics purpose [1,2]. In this respect, it is of interest to find spectral lines with convenient broadening parameters [1–5]. The $\lambda_A = 447.1$ nm neutral helium (He I) spectral line that belongs to the 4^3D–2^3P allowed transition with its $\lambda_F = 447.0$ nm forbidden component (4^3F–2^3P transition) belongs to this group of mentioned lines [2,6,7]. Namely, in the plasmas with electron densities above 4×10^{22} m^{-3} and electron temperatures above 10 000 K these line profiles merge due to the increase of the role of the Stark broadening effect [6,7]. The characteristics of this overlapping (see Fig. 1) like the ratio of the forbidden (I_F) and allowed (I_A) line maximum intensities I_F/I_A, the ratio of the dip (I_D) between both components to the maximum intensity of the allowed component I_D/I_A, the total line width of the overlapping line components ($\Delta\lambda_{1/2}$) and the wavelength distance ($\Delta\lambda_{AF}$) between the λ_A and λ_F, show a strong dependence on the electron density (N) in plasma [6,7]. Accordingly the mentioned data can be used for plasma diagnostics purpose.

These dependencies are theoretically predicted on the basis of the quasistatic approximation (G) [6] and quasistatic impact approximation (BCS) [7]. Calculations have been performed up to 40 000 K electron temperature (T). Existing measured $\Delta\lambda_{1/2}$ and $\Delta\lambda_{AF}$ values show satisfactory agreement with theoretical G and BCS data in a wide range of the electron densities $(0.4–5.0) \times 10^{23}$ m^{-3}. In the case of the I_F/I_A and I_D/I_A ratios the situation is much different (see Figs. 4 and 5). Namely, the values of these ratios, obtained experimentally, lie above the calculated values (G and BCS). The aim of this paper is to supply new experimental results to clear up this discrepancy. In this view, we have measured the overlapping profiles of the $\lambda_A = 447.1$ nm and $\lambda_F = 447.0$ nm He I

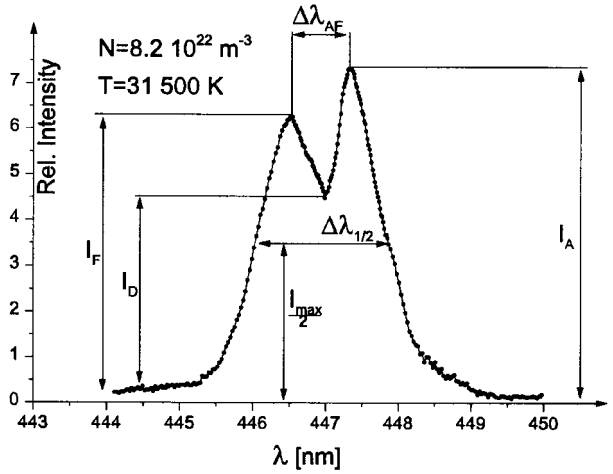

Fig. 1. The characteristics of the merged profiles of the $\lambda_A = 447.1$ nm and $\lambda_F = 447.0$ nm He I lines in the 25th μs after the beginning of the discharge recorded in decaying plasma in exp. b_1.

[a] e-mail: vladimir@ff.bg.ac.yu

spectral lines emitted under five different plasma conditions. Thus, the electron temperature has been ranged between 18 000 K and 33 000 K and the electron density between 4.4×10^{22} m^{-3} and 8.2×10^{22} m^{-3}. The found $\Delta\lambda_{1/2}$, $\Delta\lambda_{AF}$, I_F/I_A and I_D/I_A values have been compared with the existing experimental and theoretical data. On the other hand, we have monitored the 447.1 nm He I line profile during the decaying plasma up to the moment when the electron density dropped down to values with which the forbidden and the allowed components become mutually isolated. This allows us to perform measurements of the broadening characteristics of the isolated $\lambda_A = 447.1$ nm line. Our measured Stark FWHM (full-width at half maximum intensity, W) values of the $\lambda_A = 447.1$ nm line have been compared with the existing experimental and theoretical Stark width data. On the basis of the found asymmetry of the λ_A line profile we have obtained, also, the ion contribution to this line broadening (coefficients α in [1]).

2 Experiment

The modified version of the linear low pressure pulsed arc [8–11] has been used as a plasma source. A pulsed discharge was driven in a quartz discharge tube of different inner diameters (Φ): 5 mm and 25 mm and has an effective plasma length (H) from 6.2 cm to 14 cm (see Fig. 1 in [8,10]). Various dimensions of the discharge tube offer the possibility of the electron temperature variation in a wide range. The tube has end-on quartz windows. On the opposite side of the electrodes the glass tube was expanded in order to reduce the erosion of the glass wall and also the sputtering of the electrode material onto the quartz windows. The working gas was helium-nitrogen-oxygen mixture (90% He + 8% N_2 + 2% O_2) at 267 Pa and 133 Pa filling pressures in flowing regime. Spectroscopic observation of spectral lines was made end-on along the axis of the discharge tube. A capacitor of 8 μF was charged up to 4.5 kV (exp. a) and a capacitor of 14 μF was charged up to 1.5, 2.6, 3.4 and 4.2 kV, respectively (exp. b). The mentioned discharge conditions were realized in discharge tube with various lengths (H) and diameters (Φ). The used tube geometry and corresponding discharge conditions are presented in Table 1.

The line profiles were recorded by a step-by-step technique using a photomultiplier (EMI 9789 QB and EMI 9659B) and a grating spectrograph (Zeiss PGS-2, reciprocal linear dispersion 0.73 nm/mm in the first order) system. The instrumental FWHM of 0.008 nm was obtained by using the narrow spectral lines emitted by the hollow cathode discharge. The recorded profile of these lines has been of the Gaussian type within 8% accuracy in the range of the investigated spectral line wavelengths. The spectrograph exit slit (10 μm) with the calibrated photomultiplier was micrometrically traversed along the spectral plane in small wavelength steps (0.0073 nm). The averaged photomultiplier signal (five shots in each position) was digitized using an oscilloscope, interfaced to a computer. A sample output, as an example, is shown in Figures 1 and 2.

Table 1. Various discharge conditions. C-bank capacity, U-bank voltage, H-effective plasma length, Φ-tube diameter, P-filling pressure. N (in 10^{22} m^{-3}) and T (in 10^3 K) denote electron density and temperature values, respectively obtained at a 25th μs after the beginning of the discharge when the overlapping profiles were analyzed.

Exp.	C (μF)	U (kV)	H (cm)	Φ (mm)	P (Pa)	N	T
a	8	4.5	6.2	5	267	6.1	33.0
b_1	14	4.2	14.0	25	267	8.2	31.5
b_2	14	3.4	14.0	25	267	6.7	30.0
b_3	14	2.6	14.0	25	267	4.4	28.0
b_4	14	1.5	7.2	5	133	5.0	18.0

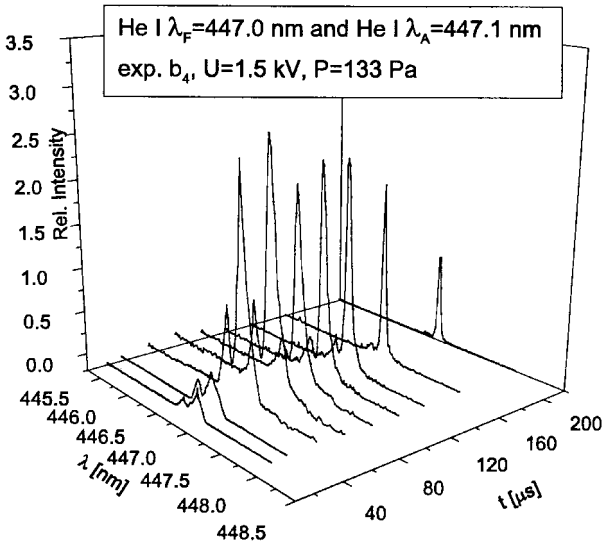

Fig. 2. Temporal evolution of the overlapping $\lambda_A = 447.1$ nm and $\lambda_F = 447.0$ nm He I spectral line profiles recorded under discharge conditions in exp. b_4.

Plasma reproducibility was monitored by the He I (501.5 nm, 388.8 nm and 587.6 nm) lines radiation and, also, by the discharge current using Rogowski coil signal (it was found to be within $\pm 5\%$).

The used deconvolution procedure in its details is described in [12]. It includes a new advanced numerical procedure for deconvolution of theoretical asymmetric convolution integral of a Gaussian and a plasma broadened spectral line profile $j_{A,R}(\lambda)$ for spectral lines. This method gives complete information on the plasma parameters from a single recorded spectral line. The method determines all broadening plasma parameters self-consistently and directly from the shape of spectral lines without any assumptions or prior knowledge. All one needs to know is the instrumental width of the spectrometer. The measured profiles were convoluted due to the convolutions of the Lorentzian Stark and Gaussian profiles caused by Doppler

Table 2. Measured overlapped profile characteristics with estimated accuracies at various N (in 10^{22} m^{-3}) and T (in 10^3 K).

N	T	$\Delta\lambda_{1/2}$ (nm)	$\Delta\lambda_{AF}$ (nm)	I_F/I_A	I_D/I_A
6.1	33.0	1.6±0.2	0.72±0.02	0.86±0.07	0.55±0.05
8.2	31.5	1.9±0.3	0.84±0.02	0.85±0.07	0.61±0.06
6.7	30.0	1.5±0.2	0.69±0.02	0.84±0.07	0.57±0.05
4.4	28.0	1.3±0.2	0.65±0.02	0.80±0.07	0.51±0.05
5.0	18.0	1.4±0.2	0.62±0.01	0.82±0.07	0.54±0.05

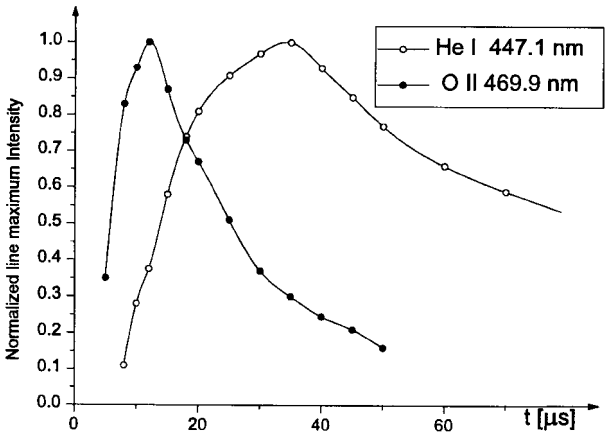

Fig. 3. Temporal evolution of the λ_A = 447.1 He I and the 469.92 nm O II spectral line maximum intensities (I_{max}) (exp. b_1).

and instrumental broadenings [1]. Van der Waals and resonance broadenings [1] were estimated to be smaller by more than an order of magnitude in comparison to Stark, Doppler and instrumental broadenings. The deconvolution procedure was computerized using the least Chi-square function [12]. The line widths were measured with ±12% accuracy and the ion contribution parameters (α) with ±15% accuracy. The plasma parameters were determined using standard diagnostics methods [13]. Thus, the electron temperature was determined from the ratios of the relative line intensities of four N III spectral lines (409.74 nm, 410.34 nm, 463.42 nm and 464.06 nm) to the 463.05 nm N II spectral line with an estimated error of ±10%, assuming the existence of the LTE [1]. In the case of the exp. b_4 the electron temperature has been obtained using the relative line intensity ratio method between the He II P_α 468.6 nm and the He I 587.56 nm lines and, also, using the ratios between the He II P_α line intensity and the five He I (388.86 nm, 471.32 nm, 501.57 nm, 667.82 nm and 706.52 nm) spectral line intensities with an estimated error of ±12%. The 388.86 nm and 501.57 nm line profiles have been corrected for the self-absorption effect using the double plasma length method described in [3]. All the necessary atomic data have been taken from [14,15]. The electron density decay was measured using a well-known single wavelength He–Ne laser interferometer technique [16] for the 632.8 nm transition with an estimated error of ±9%. The electron densities and temperatures, obtained at the moment when the overlapped line profiles were analyzed, are presented in Tables 1 and 2. This moment is selected taking into account the line maximum intensity relaxation time. We have found that the 447.1 nm He I, O II and N II spectral lines have different line maximum intensity decays. Thus, in the 25th μs after the beginning of the discharge He I line intensity reaches up to 90% of its maximum while the O II and N II line intensity maximums dropped down to 50% of their maximum (Fig. 3). Thus, the contribution of the O II line intensities to the 447.1 nm line profile at the mentioned moment can be neglected.

3 Results and discussion

3.1 Overlapping lines

Our experimentally obtained line characteristics are presented in Table 2.

In order to make the comparison easier between measured and calculated line profile parameters, their theoretical (G, BCS) dependences on the electron density are presented in Figures 4 and 5 together with the values of other authors.

Our measured $\Delta\lambda_{1/2}$ and $\Delta\lambda_{AF}$ values lie slightly below theoretically predicted ones, showing tolerable agreement with them taking into account the accuracy of measurements (see Fig. 4). Similar behavior show, also, $\Delta\lambda_{1/2}$ and $\Delta\lambda_{AF}$ values obtained in experiments [17,19,21,22, 25,27,29].

Generally, all existing experimental $\Delta\lambda_{1/2}$ and $\Delta\lambda_{AF}$ values agree with the G and BCS predictions within the uncertainties of the calculations and accuracies of the experiments (see Fig. 4).

In the case of the I_F/I_A and I_D/I_A ratios the situation is different. Our mesured values and those from [20,22,26, 28] agree with the theoretical values. But, the significant number of existing experiments give intensity ratios that overvalue the theoretical G and BCS predictions. This is particularly evident in the case of the I_D/I_A ratio (see Fig. 5).

We think that these discrepancies can be explained taking into account the role of the O II impurity ions in the plasma sources during the high current (up to 73 kA) and high temperature (up to 55 000 K) discharges. The 446.54 nm, 446.79 nm and 446.94 nm O II spectral lines originate from the high lying ($3p'''$) energy level (33.20 eV) with relatively large (0.92×10^8 s^{-1}) transition probabilities [14]. The excitation and population of this energy level take place predominantly during the recombination processes from O III states. Thus, the concentration of the O III ions ($N_{O\ III}$) is directly responsible for the mentioned O II spectral line intensities. It is known that the

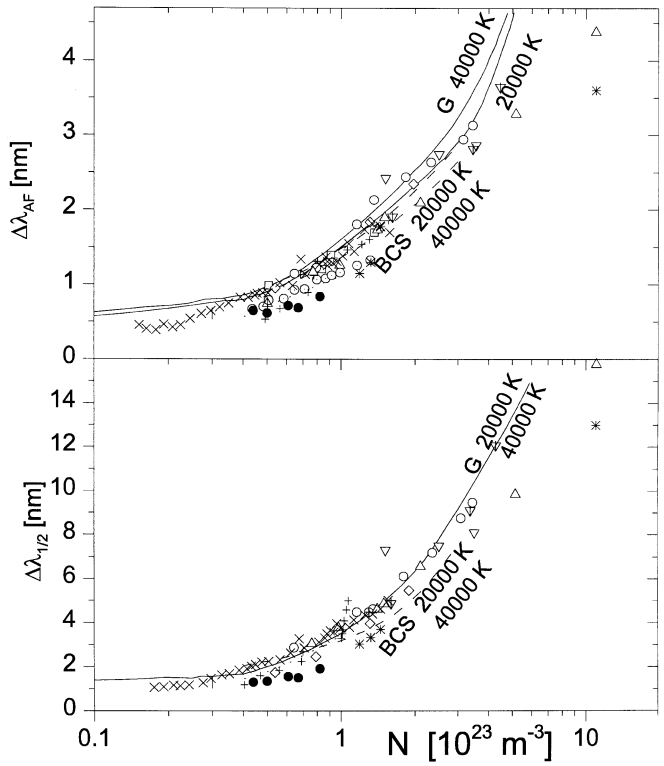

Fig. 4. The $\Delta\lambda_{1/2}$ and $\Delta\lambda_{AF}$ as a function of the electron density (N). (•) Our experimental values and those of other authors: (△) reference [17]; (□) reference [18]; (+) reference [19]; (▽) reference [20]; (⊙) reference [21]; (◇) reference [22]; (Δ) reference [23]; (◯) reference [24]; (X) reference [25]; (⊖) reference [26]; (|) reference [27]; (▽) reference [28]; (⊕) reference [31]. (- - - -) denote the best fit data from experiment [29]. Solid (G) and dashed (BCS) lines represent the calculated values by Griem [6] and Barnard *et al.* [7], respectively at 20 000 K and 40 000 K electron temperatures; * denote calculated values from [30].

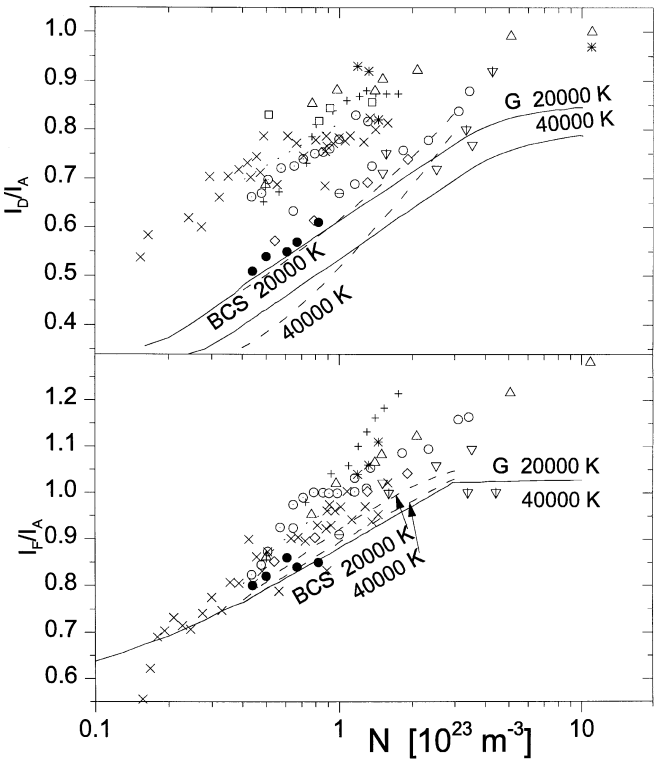

Fig. 5. The I_F/I_A and I_D/I_A as a function of the electron density (N). Symbols are the same as in Figure 4.

O III ion presence in plasma depends on the electron temperature [2]. Higher electron temperatures lead to the increase of $N_{O\ III}$ and, also, to the increase of the intensities of the mentioned O II spectral lines. In view of this, in the high temperature He plasmas [19,21,23,29], created by plasma sources with high current dicharges (up to 73 kA in [23]), the conditions to products of the oxygen atoms, and their O III and O II ions, like impurities in discharge, are fulfilled. The presence of O II ions in discharge (proportional with discharge current) may be caused by erosion mechanisms connected to the electrodes and walls of the plasma sources.

The experiments [17–19,21,23,25,29], which give higher I_F and I_D measured values, are carried out with plasmas created in the shock T-tube [18,28] and "laser focus" [17,19,21] as plasma sources. Both are known as sources where the impurity atoms can play a significant role. The presence of the O II spectral lines is explicitly confirmed in the experiments [19,22,38]. Thus, the 446.54 nm, 446.79 nm and 446.94 nm O II spectral lines lie close to the expected line center position of the forbidden He I line (λ_F) and can contribute to the increase of their intensity maximum (I_F). This position is expected at about 446.4 nm at 10^{23} m^{-3} electron density [6,7,30]. Moreover, the mentioned O II lines lie "under" the expected dip position [6,7] at about 447.0 nm between λ_F and λ_A values causing higher measured I_D values in comparison with the calculated I_D values. The mentioned O II lines have a negligible influence on the intensity of the allowed λ_A line expected at 447.7 nm [6,7,30]. Hence the possible presence of the O II lines results in the increase of the measured I_F/I_A and I_D/I_A values so that these go up above the theoretical predictions. This discrepancy between the measured and calculated intensity ratios must increase with the density of O II ions (at higher T and N). On the other hand, the influence of the mentioned O II lines on the $\Delta\lambda_{1/2}$ and $\Delta\lambda_{AF}$ values is practically negligible.

It turns out that a number of experimental [32–38] and theoretical [39–45] works are devoted to the 447.1 nm He I line profile investigations at an electron density below 3×10^{22} m^{-3}. The smearing of the central dip is, with these plasma compositions and electron density, explained by taking into account the ion dynamic effect. The ion dynamic effect depends on the mass (μ) and tempereture (T_i) of the perturbing ions expressed as $(T_i/\mu)^{1/2}$. With our plasma conditions and compositions this effect is negligible [2,12,44].

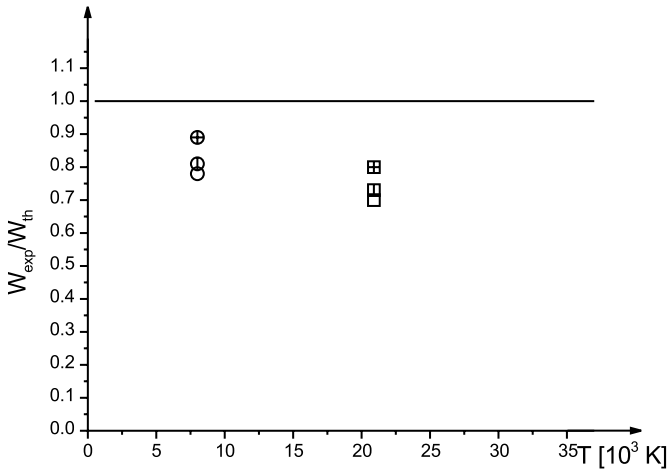

Fig. 6. Ratios of the experimental total half-width ($W_{\rm exp}$) of the separated $\lambda_{\rm A} = 447.1$ nm He I spectral line to the various theoretical ($W_{\rm th}$) predictions *vs.* electron temperature. Circle and square represent our experimental data and those from [48], respectively. Empty, half and quartal divided symbols represent the ratios related to the theories taken from [1,46,47], respectively.

3.2 Separated lines

We have monitored the line profile up to the 120th μs (see Fig. 2) after the beginning of the discharge (in exp. b_4) when the electron density has dropped down to $(6.0 \pm 0.6) \times 10^{21}$ m^{-3} and the electron temperature to (8 000 $\pm$ 2 000) K. 6 000 K temperature of the emitting atoms, at this moment, was found due the Gauss component in convolutions [12]. With these plasma parameters the $\lambda_{\rm A}$ can be used as isolated line. Applying the deconvolution procedure described in [12] we have obtained the following line profile characteristics: total line width (electron + ion) $W_{\rm t} = 0.203$ nm; electron width $W_{\rm e} = 0.102$ nm; ion contribution parameter normalized to 10^{22} m^{-3} electron density, $\alpha = 0.937$. Our ion contribution parameter is higher than the one obtained in [1] ($\alpha = 0.625$) and [46] ($\alpha = 0.650$).

In Figure 6 the ratios $W_{\rm exp}/W_{\rm th}$ are presented *versus* electron temeperature. Our experimental data and those from [48] are related to the theoretical predictions taken from [1,46,47].

The experimental results lie below all three theoretical predictions. Our mesured $W_{\rm exp}$ fairly agrees (within 12%) with theoretical data from [47].

4 Conclusion

We have obtained agreement between our measured line characteristics and their calculated values on the basis of the quasistatic approximation [6,7]. As possible explanation of the disagreement between some experimental results and theoretical predictions in the case of the line intensity ratios we have recommended the possible role of the O II impurity ions.

On the basis of the asymmetry of the $\lambda_{\rm A}$ line profile we have obtained, also, the ion broadening parameter which is about 50% higher than the existing theoretical values.

This research is a part of the project supported by the Ministry of Science and Development of the Republic of Serbia.

References

1. H.R. Griem, *Spectral Line Broadening by Plasmas* (New York, Acad. Press, 1974).
2. H.R. Griem, *Principles of Plasma Spectroscopy* (Univ. Press Cambridge, Cambridge, 1997).
3. N. Konjević, Phys. Rep. **316**, 330 (1999).
4. S. Djeniže, Phys. Scripta **61**, 412 (2000).
5. V. Milosavljević, M.S. Dimitrijević, S. Djeniže, Astrophys. J. Supp. **134**, (2001, in press).
6. H.R. Griem, Astrophys. J. **154**, 1111 (1968).
7. A.J. Barnard, J. Cooper, L.J. Shamey, A&A **1**, 28 (1969).
8. S. Djeniže, A. Srećković, J. Labat, R. Konjević, L.Č. Popović, Phys. Rev. A **44**, 410 (1991).
9. S. Djeniže, A. Srećković, J. Labat, M. Platiša, Z. Phys. D **21**, 795 (1991).
10. S. Djeniže, V. Milosavljević, A. Srećković, JQSRT **59**, 71 (1998).
11. V. Milosavljević, S. Djeniže, M.S. Dimitrijević, L.Č. Popović, Phys. Rev. E **62**, 4137 (2000).
12. V. Milosavljević, G. Poparić, Phys. Rev. E **63**, 036404 (2001).
13. R. Rompe, M. Steenbeck, *Ergebnisse der Plasmaphysik und der Gaselektronik* (Akademie Verlag, Berlin, 1967)
14. W.L. Wiese, M.W. Smith, B.M. Glennon, *Atomic Transition Probabilities* (DC. US. Govt. Print. Office, Washington, 1966), NSRDS NBS 4, Vol. 1.
15. S. Glenzer, H.J. Kunze, J. Musielok, Y. Kim, W. Wiese, Phys. Rev. A **49**, 221 (1994).
16. D.E.T.F. Ashby, D.F. Jephcott, A. Malein, F.A. Raynor, Appl. Phys. **36**, 29 (1965).
17. R.J. Hawryluk, G. Bekefi, E.V. George, Phys. Rev. A **10**, 265 (1974).
18. J.D. Hey, H.R. Griem, Phys. Rev. A **12**, 169 (1975).
19. G. Baravian, J. Bretagne, J. Godart, G. Sultan, Z. Phys. B **20**, 255 (1975).
20. R. Okasaka, M. Shiumizu, K. Fukuda, J. Phys. Soc. Jap. **43**, 1708 (1977).
21. B.T. Vujičić, Lj. Ćirković, Fizika (Zagreb) **16**, 201 (1984).
22. N.I. Uzelac, N. Konjević, Phys. Rev. A **33**, 1349 (1986).
23. H. Suemitsu, K. Iwaki, Y. Takemoto, E. Yoshida, J. Phys. B **23**, 1129 (1990).
24. N.I. Uzelac, I. Stefanović, N. Konjević, JQSRT **46**, 447 (1991).
25. C. Perez, I. de la Rosa, J.A. Aparicio, S. Mar, M.A. Gigosos, Jpn J. Appl. Phys. **35**, 4073 (1996).
26. V. Milosavljević, S. Djeniže, Proceed. of the 24th ICPIG Warshawa, Poland **P II**, 19 (1999).
27. H. Wulff, Z. Phys. **150**, 614 (1958).
28. J.R. Greig, L.A. Jones, R.W. Lee, Phys. Rev. **9**, 44 (1974).
29. R.H. Nelson, A.J. Barnard, JQSRT **11**, 161 (1971).
30. J.C. Valognes, J.P. Bardet, JQSRT **56**, 855 (1996).
31. H.F. Berg, A.W. Ali, R. Lincke, H.R. Griem, Phys. Rev. **125**, 199 (1962).

32. D.D. Burgess, C.J. Cairns, J. Phys. B **3**, L67 (1970).
33. J.W. Birkeland, M.E. Bacon, W.G. Braun, Phys. Rev. A **3**, 354 (1971).
34. H.W. Drawin, J. Ramette, Z. Naturforsch. **29a**, 838 (1974).
35. C. Fleurier, G. Couland, J. Chapelle, Phys. Rev. A **18**, 575 (1978).
36. C. Fleurier, G. Couland, J. Chapelle, Physica C **100**, 127 (1980).
37. V. Helbig, H. Ehrich, in *Spectral Line Shapes*, edited by B. Wende (de Gruyter, Berlin, 1981), p. 179.
38. A. Piel, H. Richter, Z. Naturforsch. **38a**, 37 (1983).
39. D.D. Burgess, J. Phys. B **3**, L70 (1970).
40. R.W. Lee, J. Phys. B **6**, 1044 (1973).
41. A.J. Barnard, J. Cooper, E.W. Smith, JQSRT **14**, 1025 (1974).
42. A. Brissaud, C. Goldbach, J. Leorat, A. Mazure, G. Nollez, J. Phys. B **9**, 1147 (1976).
43. D. Voslamber, E.R.A. Segre, JQSRT **25**, 45 (1981).
44. A. Calisti, R. Stamm, B. Talin, Phys. Rev. A **38**, 4883 (1988).
45. T. Schöning, J. Phys. B **27**, 4501 (1994).
46. J.M. Bassalo, M. Cattani, V.S. Walder, JQSRT **28**, 75 (1982).
47. M.S. Dimitrijević, S. Sahal-Bréchot, A&A Supp. Ser. **82**, 519 (1990).
48. D.E. Kelleher, JQSRT **25**, 191 (1981).